Infants and young children modeling method for numerical dosimetry studies: application to plane wave exposure

You may also be interested in:

A comprehensive tool for image-based generation of fetus and pregnant women mesh models for numerical dosimetry studies
S Dahdouh, N Varsier, A Serrurier et al.

Exposure assessment of one-year-old child to 3G tablet in uplink mode and to 3G femtocell in downlink mode using polynomial chaos decomposition
I Liorni, M Parazzini, N Varsier et al.

Influence of pregnancy stage and fetus position on the whole-body and local exposure of the fetus to RF-EMF
N Varsier, S Dahdouh, A Serrurier et al.

Analysis of RF exposure in the head tissues of children and adults
J Wiart, A Hadjem, M F Wong et al.

Variability analysis of SAR from 20 MHz to 2.4 GHz for different adult and child models
E Conil, A Hadjem, F Lacroux et al.

SAR and induced currents in adults and children exposed to EAS devices
M Martínez-Búrdalo, A Sanchis, A Martín et al.

Infants and young children modeling method for numerical dosimetry studies: application to plane wave exposure

S Dahdouh[1,2]**, N Varsier**[2,3]**, M A Nunez Ochoa**[2,3,4]**, J Wiart**[1,2]**, A Peyman**[5] **and I Bloch**[1,2]

[1] LTCI, CNRS, Télécom ParisTech, Université Paris Saclay, Paris, France
[2] Whist Lab, Paris, France
[3] Orange Labs, Issy les Moulineaux, France
[4] Institut Mines-Telecom, Telecom Bretagne, Brest, France
[5] Center for Radiation, Chemicals and Environmental Hazards, Public Health England, Chilton, Didcot, UK

E-mail: sonia.dahdouh@gmail.com and isabelle.bloch@telecom-paristech.fr

Abstract

Numerical dosimetry studies require the development of accurate numerical 3D models of the human body. This paper proposes a novel method for building 3D heterogeneous young children models combining results obtained from a semi-automatic multi-organ segmentation algorithm and an anatomy deformation method. The data consist of 3D magnetic resonance images, which are first segmented to obtain a set of initial tissues. A deformation procedure guided by the segmentation results is then developed in order to obtain five young children models ranging from the age of 5 to 37 months. By constraining the deformation of an older child model toward a younger one using segmentation results, we assure the anatomical realism of the models. Using the proposed framework, five models, containing thirteen tissues, are built. Three of these models are used in a prospective dosimetry study to analyze young child exposure to radiofrequency electromagnetic fields. The results lean to show the existence of a relationship between age and whole body exposure. The results also highlight the necessity to specifically study and develop measurements of child tissues dielectric properties.

Keywords: infants modeling, anatomy transfer, numerical dosimetry, plane wave exposure

(Some figures may appear in colour only in the online journal)

1. Introduction

The rise of new technologies for mobile communication such as bluetooth, WiFi or LTE and the advent of smartphones have raised the need to further study the impact of radiofrequency (RF) electromagnetic fields on the human body. These developments are changing common practices, and very young children, without necessarily being directly users of wireless systems, are now placed in configurations (e.g. in the arms of calling parents) where they are exposed to radio frequency electromagnetic fields (RF-EMF). To assess the exposure of infants and young children, RF-EMF simulations on realistic numerical models of the young child are used to compute the specific absorption rate (SAR) (Wiart *et al* 2008).

While adult modeling has been intensively studied (Wiart *et al* 2008, Xu and Eckerman 2009) using either mathematical, voxelized or synthetic methods, and fetal and pregnant woman modeling has been the focus of several studies such as Dahdouh *et al* (2014), few authors have addressed the problem of infants and really young children modeling. Most of the studies on the young children are concentrated on the exposure for children above the age of four years (Wiart *et al* 2008), and very few have addressed the issue of infants modeling and exposure assessment. To the best of our knowledge, this paper presents the first study that addresses both problems simultaneously.

Most of the available young children models (below the age of three years) can be separated into three different categories: (I) the ones obtained through a purely manual segmentation, (II) the ones obtained purely synthetically, and finally (III) the ones obtained by downsizing older children or adults models. While purely manual segmentation as in Li *et al* (2015) allows for the construction of accurate children models, the amount of manual processing is cumbersome and prevents the use of such a methodology at a larger scale. A realistic 8 weeks old model has been built synthetically in Lee *et al* (2007). Purely synthetic models, such as the one proposed in Cassola *et al* (2013), are difficult to evaluate since anatomical realism is difficult to guarantee, but have the advantage of proposing a framework to build new models to be able to cover a wider age range. Older children and adults downsizing has been used in Hadjem *et al* (2005), Nagaoka *et al* (2008) for example, but they usually fail to take precisely into account the different anatomical variabilities that exist when comparing adults to infants (Wiart *et al* 2008, Li *et al* 2015). Moreover, head models of children not younger than 5 years old are mostly proposed. Recently, an 8 weeks old infant model has been added to the *virtual population* (Gosselin *et al* 2014) and is actually a morphed version of the 5 years old female child.

In order to overcome all the issues cited above, this paper proposes a new infant modeling framework that combines automatic segmentation on 3D MRI infant data with an anatomy transfer framework based on the segmentation results. This allows us to overcome the usual drawbacks of the scaling or morphing methods, alleviates the burden of purely manual segmentation, and allows for the construction of realistic anatomical models at any age if imaging data, typically magnetic resonance imaging (MRI), of a patient at the target age are available.

Whole body MRI data are difficult to obtain for young children (due to ethical as well as technical limitations) and they usually display strong artifacts such as motion, low resolution and strong partial volume effect. Due to the possible deleterious effects, other modalities such as CT-scan are nearly never used in this young population and such data are not easily available. This makes MRI the logical choice for the development of the method. While research on multi-organs CT scans segmentation methods is an extensively explored field, few authors have addressed the problem of multi-organs segmentation for abdominal or whole body MRI data and to our knowledge no method exists to automatically generate young children models from partially segmented data.
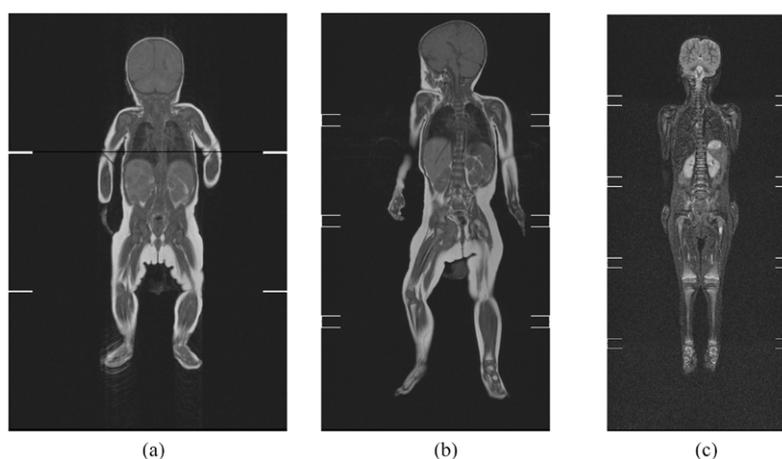
Figure 1. Slices of three 3D MRI volumes of young children at different ages (a) 5 months (b) 2 years 1 month (c) 3 years 1 month.

Facing the need to deal with the automatic segmentation of low quality MRI data as well as deriving whole body models from this segmentation, the aim of this paper is to combine segmentation and anatomy transfer to build reliable body models from low resolution data using anatomical information as prior. While other papers rely heavily on manual segmentation, the aim of this paper is to automate both the segmentation and the modeling parts, and to propose a reliable framework to automatically generate children whole body models. Once done, these models will be used to assess the young children exposure to plane waves from birth to the age of 3 years old.

The contributions of this paper are twofold; first a new framework gathering segmentation, a new anatomy transfer method and 3D modeling to build realistic young children 3D models is proposed; secondly, a preliminary dosimetry study on these data is performed. Data are described in section 2. The first part of section 3 focuses on the development of a multi-organs segmentation framework for MRI data. The proposed anatomy transfer method is then described and resulting child models are presented. Finally, section 4 focuses on an analysis of the exposure of the young child to radio-frequency electromagnetic fields.

2. Medical data

As detailed next, five MRI volumes imaging children with ages ranging from 5 to 37 months old are used. Figure 1 contains examples of three slices of three different MRI volumes. Table 1 sums up the main characteristics of the used data sets. MRI images are T1 weighted in four cases and T2 weighted in the last one. Additionally, an existing mesh model of an 8 years old child was used for the anatomy transfer (see section 3.2). To reduce acquisition time, the imaging data are strongly anisotropic, with a very good in-slice resolution but a large slice thickness. All the images were recorded on children during medical examinations as part of the clinical routine and parents were asked to give their informed consent for the use of the data for research purposes.

Since all the structures and tissues of interest are not visible and easily segmented on the available data, a child model construction pipeline was designed to build, and then further enrich, children models.

Table 1. Image Database.

Modality	Age	Slice thickness (mm)	Image resolution (mm px^{-1})	Structures of interest
MRI T1	5 months	7	0.634	envelope + brain + lungs + spleen + liver + kidneys
MRI T1	1 year 5 months	7	0.966	envelope + brain + lungs + spleen + liver + kidneys
MRI T1	2 years 1 month	7	0.966	envelope +brain + lungs + spleen + liver + kidneys
MRI T1	2 years 3 months	7	0.755	envelope +brain + lungs + spleen + liver + kidneys
MRI T2	3 years 1 month	7	0.94	envelope + brain + lungs + liver + kidneys
Mesh model Christ *et al* (2010)	8 years	NA	NA	66 tissues

3. Infants and children models construction

3.1. Semi-homogeneous models construction from whole body MRI data

In order to model infants and young children, a multi-organs framework for simultaneously segmenting different tissues in 3D MRI data has been developed in Dahdouh and Bloch (2015). This method extends the Variational Region Growing segmentation framework proposed in Rose *et al* (2009) and Revol-Muller *et al* (2012), which integrates a shape prior in the region growing process. The approach proposed here integrates multiple shape constraints into a multi-region growing segmentation framework and proposes a new intensity criterion for segmenting noisy data. More precisely, to compensate for the low resolution and the lack of contrast, the segmentation framework is performed on a graph of supervoxels computed using the SLIC algorithm (Achanta *et al* 2012), and a shape prior per tissue, represented by its Legendre moments, is used. Both local (the supervoxel value) and global (neighboring regions mean intensity values, adjacent supervoxels values and distance to the neighboring regions) information is used to compute the intensity-based energy, given by the following equation.

Let Ω be a bounded and open subset of $\mathbf{R}^3$ and $I : \Omega \to \mathbf{R}$ an image. Ω_{in}^i represents the segmented region i and is a subset of Ω, Φ_i represents the characteristic function of the evolving region i and Φ_i^n, the characteristic function at iteration n.

The intensity-based energy is defined as:

$$J_{\mathrm{image}}(\Phi_i^n) = \sum_{x\in\Omega}\left((|I(x)-\mu_i|)^2 + \frac{1}{N_{aj_x}}\sum_{y\in aj_x}(|I(y)-\mu_i|)^2\right).\Phi_i^n(x)$$

$$+ \sum_{x\in\Omega}\left(\sum_{r\neq i}\lambda(x,r)(|I(x)-\mu_r|)^2 + \frac{1}{2N_{aj_x}}\sum_{y\in aj_x}\sum_{r\neq i}\lambda(y,r)(|I(y)-\mu_r|)^2\right).(1-\Phi_i^n(x))$$

with μ_i the mean gray level value of region i, computed at each iteration, aj_x the set of adjacent nodes to x, of cardinality N_{aj_x} and $\lambda(x,r)$ a weighting function to take into account the spatial proximity of all the other regions into the image.

Additionally, a shape prior per organ is used to constrain the segmented organ toward its actual shape. Learned from a set of annotated images, it is added as an energy term in the

Figure 2. Child semi-homogeneous model construction. Reconstruction of five models based on the automatic segmentation of soft-tissues in MRI data.

functional to be optimized. Shape priors are meshed and registered to the growing regions using the shape matching method proposed in Guy *et al* (2014).

Inter-regions conflicts resolution is handled using a weighted Voronoi decomposition method, the weights being determined by the magnitude ratio of tissues densities. The energy terms of the global energy equation are weighted using an information on growth direction and on gradient vector flow value. The aim is to either guide the segmentation toward the image natural edges if it is consistent with image and shape prior terms, or to enforce the shape prior term otherwise. Results on 3D infants MRI data were presented in Dahdouh and Bloch (2015) and compared to a set of manual segmentations. Both visual comparison and quantitative measurements showed good results with a mean Dice index (similarity measurement) of 0.81 for the simultaneous segmentation of five tissues. Finally, the envelope is segmented using a thresholding approach and refined manually.

The segmentation method has been applied to the whole set of 3D MRI data and five semi-homogeneous models of children have been obtained as shown in figure 2.

The aim of this paper being to develop reliable models for dosimetry studies, the need to enrich the obtained models with tissues such as muscles, fat or bones in order to obtain more heterogeneous ones has arised. However, the data being of low quality, further segmentation was not possible and an alternative strategy had to be developed, as detailed next.

3.2. Models enrichment: anatomy transfer framework

While many authors have addressed the problem of realistic anatomical simulation and deformation (Faraj *et al* 2012, Ali-Hamadi *et al* 2013), few methods have been developed so far to deal with automatic anatomy modeling or anatomy transfer from one character to another. To our knowledge, one of the only works addressing this problem is Ali-Hamadi *et al* (2013), where a semi-automatic method was proposed for transferring the internal anatomy of a highly-detailed anatomical model to a minimal model composed of only skin. Skin layers are first registered and a fat layer is manually added. A semi-automatic method to generate this fat layer is proposed and a Laplacian deformation guided by anatomical constraints is used to transfer bones, muscles, viscera and skeleton. As stated by the authors, one of the drawbacks of using direct Laplacian interpolation is the apparition of artifacts when transferring

the whole anatomy as well as the skeleton. Moreover, the authors were dealing with data and meshes of high quality, which is not our case. Due to low resolution of data available in this study, details on hands, feet (such as fingers or toes separation or even their positioning) and facial details (such as eyes position or nose) are missing. These artifacts are not consistent in all the data, which means that we had to develop a method robust enough to deal with artifacts varying from one model to another. In order to bypass the shortcomings of the method proposed in Ali-Hamadi *et al* (2013), the authors suggested to take advantage of more anatomical knowledge to constrain the deformation process, which is one of the keypoints of the method proposed here.

As detailed in the following, a novel deformation framework guided by the segmentation results obtained in Dahdouh and Bloch (2015) is proposed here. The segmented tissues will be used as a prior to anchor and guide the deformation of the other surrounding tissues.

3.2.1. Overview. The model enrichment framework takes as input a set of 2-manifold triangle meshes (i.e. a list of polygones indexed over a list of vertices) to be used as reference tissues for the anatomy transfer, as well as a set of 2-manifold triangle meshes representing the existing tissues of the model to enrich. The *Eartha* model of the *virtual family* (Christ *et al* 2010) has been used here as reference and deformed toward the target ages and models.

During the first step, a topology unification procedure is applied between the existing soft-tissue and skin meshes of the target model and their corresponding counter-parts in the reference model. The reference skeleton is then deformed toward the target child model using the previously registered skin and soft tissues as prior. Finally, the remaining reference tissues are incrementally deformed from the reference to the target model using the previous tissues deformations as constraints.

3.2.2. Topology unification. The aim of our deformation method is to transfer a whole anatomy from a source model to a target one, using only the skin model and few organs of the target as anchors. The first step is to establish vertex correspondence between both skin and soft-tissues models. Since they belong to different subjects, they have different topologies and positions.

Soft tissues correspondence. The source brain, lungs and liver are first deformed toward the target ones using a global PCA registration computed on the normal field of each mesh. The scaling factor used is based on the longest geodesic distance of each source mesh. All the pairwise registrations between source and target tissues are then refined using an iterative closest point algorithm (Besl and Mckay 1992). Using this procedure, topologically similar soft-tissue meshes at all studied ages are generated.

Skin registration. The same global procedure is first applied to register source and target skin meshes. However, due to the high variability in terms of positioning and shape, it was not enough to ensure a correct registration. Indeed, while body position is usually fixed when dealing with adults MRI, in the case of young children, motion is often an issue, and the body position can thus vary from one patient to another. It means that head and limbs positions can vary greatly from one model to another. To address the head positioning issue, a Moving Least Square (MLS) based deformation using the method proposed in Zhu and Gortler (2007) and a Euclidean distance for weights computation is applied. Euclidean distance is preferred here to the geodesic like distance proposed in Zhu and Gortler (2007) since landmarks are nodes of the soft tissue meshes and thus do not belong to the skin mesh. A set of random landmarks selected on both source and target brain models is used to deform the head, and a set of

randomly selected landmarks on lungs and liver source and target meshes is used to anchor the rest of the body. As in Ali-Hamadi *et al* (2013) and Gilles *et al* (2010), the final skin surface is obtained using the shape matching deformation method proposed in Müller *et al* (2005) which is achieved using a closest point correspondence procedure and a smooth as rigid as possible deformation field based on these correspondences. This three steps procedure allows us to successfully register a source skin model of an 8 years old child toward skin models of different children at different ages and positions. While some artifacts remain in the skin registration result (mainly around the hands and the feet when the initial segmentation was too rough), the result is satisfying enough to guide the rest of the deformation procedure as explained next.

3.2.3. Skeleton deformation. The skeleton Sk is divided into 21 bones $Sk(i), i \in \{1..21\}$, and $Sk = \cup_{i=1}^{21} Sk(i)$. Using a set of random landmarks selected on registered soft tissues and skin models, a semi-rigid MLS deformation, based on the method of Zhu and Gortler (2007) and a Euclidean distance, is used to deform each $Sk(i)$ bone towards its target position. The use of landmarks on internal tissues in addition to the landmarks on skin constrains the deformation, allowing us to limit the non realistic bending and stretching observed in Ali-Hamadi *et al* (2013).

3.2.4. Soft tissues transfer. Once the skin *Env*, brain *Br*, lungs *Lg*, liver *Lv* and skeleton *Sk* are deformed toward the target position and shape as explained above, the other tissues are iteratively registered. The registration order is depending on the distance between the heart and the considered tissue, going outward toward the skin. Each registered tissue is then added as a constraint to the other tissues to be deformed. This allows us to not model fat beforehand as was done by Ali-Hamadi *et al* (2013) since its registration will be dependent on the registration of the other tissues. Each tissue is deformed using a MLS based procedure using randomly selected points on all the already registered tissues, as explained in algorithm 1.

Algorithm 1: Soft tissues transfer

Data: $s\_Sk(i)_{i \in \{1..21\}}$: $Sk(i)$ of the source skeleton, $t\_Sk(i)_{i \in \{1..21\}}$:
registered $Sk(i)$ of the target skeleton, $s\_Env, t\_Env, s\_Br, t\_Br,$
s_Lg, t_Lg, s_Lv, t_Lv of the source and registered target models,
$s\_Tiss(k)_{k \in \{1..5\}}$

$m\_points \leftarrow$ Select 50 random vertices on each $s\_Sk(i), s\_Env, s\_Br, s\_Lg, s\_Lv$

$d\_points \leftarrow$ Get equivalent vertices on each $t\_Sk(i), t\_Env, t\_Br, t\_Lg, t\_Lv$

Sort $s\_Tiss(k)_{k \in \{1..5\}}$ by increasing distance to $s\_Sk(i)$

foreach $s\_Tiss(k)_{k \in \{1..5\}}$ **do**

    $t\_Tiss(k) \leftarrow$ Deform $s\_Tiss(k)$ using m_points and d_points in a MLS procedure using a Euclidean distance

    $sp\_points \leftarrow$ Select 50 random vertices on $s\_Tiss(k)$

    $tp\_points \leftarrow$ Get equivalent vertices on $t\_Tiss(k)$

    $m\_points \leftarrow m\_points \cup sp\_points$

    $d\_points \leftarrow d\_points \cup tp\_points$

end

Thirteen tissues have been deformed at once allowing us to obtain detailed and accurate child models with ages ranging from 5 months to 3 years. Results of the whole deformation pipeline are illustrated in figure 3.

(a)   (b)   (c)   (d)
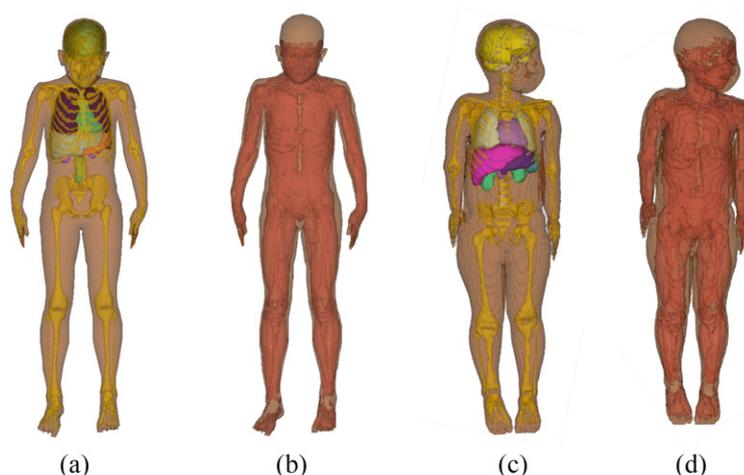
Figure 3. Source eight years old female model (a) skin, skeleton and soft tissues, and (b) skin and muscles, deformed towards a (c-d) 2 years 1 months old child model. (Scales are different for the two models.)

Table 2. Comparison between average French child weights and numerical child model weights in kg.

| Model | Ref. values for F | | Ref. values for M | | Model weight |
	Avg.	97th perc.	Avg. weight	97th perc.	
5 months	7	9	7	9.2	8
18 months	10.2	13	11	13.5	11.9
2 years	11.5	14.5	12.2	15	18.38
3 years	14	18	14.5	18	14.09

Note: The weights of the four different numerical models were computed using different tissue densities per age (F for female and M for male).

4. Children exposure to plane waves: preliminary dosimetry results

In 2013, a USA *Common Sense Media* research study highlighted the fact that 75% of American children have access to smart wireless devices like smartphones and tablets at home, and that up to 38% of children under the age of two have already used a smart mobile device for playing games or watching videos. This raises the question of the impact of such exposure on young children, and the World Health Organization (WHO) has dubbed numerical EMF dosimetry studies on children as a high priority. However, so far, no study has been published analyzing the exposure of very young children. Indeed, the specific morphological changes in very young children, the deployment of new technologies and the rapid evolution of usages are major challenges for the assessment of RF-EMF exposure. As a prelimiray answer to this question, we analyzed in this paper the environmental exposure of very young children to RF-EMF by using three (selected as described next) of the five developed whole body children models described in the previous sections.

As a first step, the realism of the developed models has to be studied. Then, the exposure of children models to plane waves is analyzed. Finally, the importance of using age specific dielectric properties for the analysis of the exposure of very young children is discussed.

Table 3. Dielectric properties of the 5 and 18 months old children tissues.

Tissue	2100 MHz				2600 MHz			
	5 months child		18 months child		5 months child		18 months child	
	P	C (S/m)	P	C (S/m)	P	C (S/m)	P	C (S/m)
Lungs (1)	49.16	1.36	49.16	1.36	48.17	1.79	48.17	1.79
Liver (2)	43.94	1.37	43.94	1.37	42.79	1.79	42.79	1.79
Kidneys (3)	54.02	2.05	54.02	2.05	52.41	2.55	52.41	2.55
Heart (4)	55.96	1.87	55.96	1.87	54.51	2.38	54.51	2.38
Spleen (5)	53.52	1.87	53.52	1.87	52.17	2.35	52.17	2.35
Stomach (6)	62.99	1.80	62.99	1.80	61.92	2.34	61.92	2.34
Brain (7)	58.12	1.53	42.86	1.15	57.29	2.04	42.05	1.57
CSF (8)	67	3.03	67	3.03	66.02	3.60	66.02	3.60
Homog. tissues (9)	55.55	2.79	55.55	2.79	54.13	3.29	54.13	3.29
Fat (10)	13.93	0.38	13.93	0.38	13.65	0.51	13.65	0.51
Muscle (11)	60.38	1.78	47.04	1.49	59.36	2.35	45.85	2.05
Skeleton (12)	24.57	2.88	24.57	2.88	23.61	3.86	23.61	3.86
Skin (13)	38.87	1.14	29.38	0.91	38.2	1.5	28.64	1.25
Skull (14)	29.63	0.87	16.26	0.49	28.79	1.17	15.64	0.68

4.1. Children's voxel models construction and validation

The children models are first rasterized and four (one per age) $1 \times 1 \times 1 \, \text{mm}^3$ voxel models are built. To validate the proposed models, their simulated weights are compared to the reference values from the World Health Organization (WHO) child growth standards as described in table 2. To compute these weights, the tissue densities from Duck (1990) were used. The weight of all tissues at all ages are given in appendix. Since all tissues have not been modeled, a unique density value (intestine), known to approximate well homogeneous tissues, has been chosen for the missing tissues. Despite this approximation, the computed weights remain within the bounds of acceptable weights with regard to the WHO standards, for all models except the 2 years old model whose weight is above the 97th percentile leading us to discard it for the numerical dosimetry analysis. As an additional validation, the realism of the models was positively appreciated by medical experts.

4.2. Numerical dosimetry study design

Each of the three children models was exposed to a frontal plane wave vertically polarized at 2100 and 2600 MHz (classical configurations corresponding to 3 G and 4 G, respectively). As most of the adults' studies have been performed on floating models, we decided here to do the same to be able to more easily draw comparisons between children and adults results.

4.2.1. Dielectric properties. Numerous studies have assessed the existence of an age variation of dielectric properties of some tissues (Peyman *et al* 2001, Gabriel 2005, Peyman and Gabriel 2010). We therefore decided to use the dielectric properties (permitivity P and conductivity C (S/m)) specific at 2100 and 2600 MHz for the child tissues when a significant age-based variation was reported, and the adult's values when no age-based variation was reported. Precise values are still not completely known, and interpolated from equivalent tissues from animals and adults. When available, dielectric properties were derived from 30 days old rats dielectric properties (Peyman *et al* 2001). When tissues showed a relevant age-based variation, tissues properties were derived from 10 kg pigs (Peyman and Gabriel 2010). Otherwise, they were derived from adult sheep dielectric properties (Gabriel *et al* 1996). Table 3 details the

Table 4. *WBSAR* and *SAR*10*g* at 2100 (3 G) and 2600 (4 G) MHz for each child model (Values have to be multiplied by 10^{-05}).

	5 months	18 months	3 years
WBSAR − 3*G*	2.041	2.061	1.812
WBSAR − 4*G*	2.084	2.039	1.832
*SAR*10*g* − 3*G*	26.09	14.99	15.08
*SAR*10*g* − 4*G*	17.99	15.65	15.78
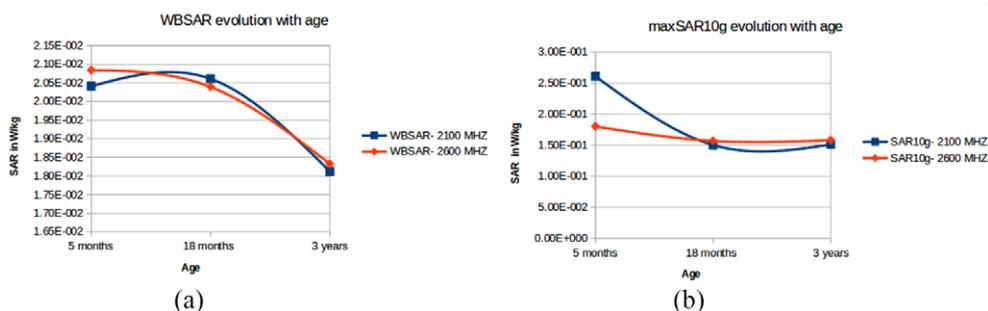
Figure 4. (a) WBSAR and (b) maxSAR10g evolution with age at 2100 and 2600 MHz.

dielectric properties of the different tissues at both frequencies for two of the children models. Since values at 37 and 18 months are similar, the same dielectric properties are used for both ages. As for densities, the homogeneous tissue was given the same dielectric properties as the intestine, as the best average equivalent values. It has to be noted that the precise estimation of all values at all ages is to a large extent an open question.

4.2.2. SAR computation. Two far-field exposure scenarios were considered using an incident plane wave, polarized vertically, with a frontal incidence, emitting at 2100 MHz and 2600 MHz. The total power absorbed by the children and the Specific Absorption Rate (SAR) distributions (in W kg^{-1}) were evaluated using the well-known Finite Difference Time-Domain (FDTD) method (Taflove 2005). In this paper, we computed the whole body SAR (*WBSAR*), the maximum SAR averaged over 10 grams of tissues (*SAR*10*g*) and average SAR values in specific organs of the child models. All the calculated values were estimated for an incident E-field of 1 V m^{-1}.

4.3. Numerical dosimetry study results

4.3.1. Analysis of the EMF exposure evolution with age for very young children. Results of the children exposure in terms of *WBSAR* and *SAR*10*g* are given in table 4 and illustrated in figure 4.

As we can see, *WBSAR* exhibits the same behavior for both frequency bands: stable between 5 and 18 months and decreasing afterwards. On the other hand, the *SAR*10*g* decreases only slightly between 5 and 18 months and remains stable afterwards.

However, these results have to be taken cautiously and further analysis with more models has to be performed to be able to draw definite conclusions. Moreover, to interpret the *SAR*10*g* results, we should keep in mind that the maximum can occur at different locations depending on the model. The amount of subcutaneous fat may also influence the results.

Table 5. WBSAR and maxSAR10g values when using child specific dielectric properties (CDP) and adult dielectric properties (ADP) for the 18 months child model at 2100 and 2600 MHz.

Value	2100 MHz		2600 MHz	
	CDP	ADP	CDP	ADP
WBSAR	2.06	2.04	2.04	2.04
maxSAR10g	15.0	14.9	15.7	15.2

Note: values have to be multiplied by 10^{-05}.
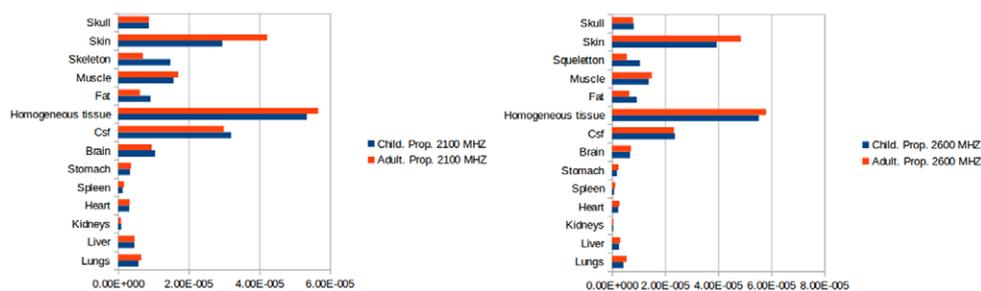
Figure 5. Comparison between local average SAR values obtained for child (blue) and adult's (red) dielectric properties. Left: 2100 MHz. Right: 2600 MHz.
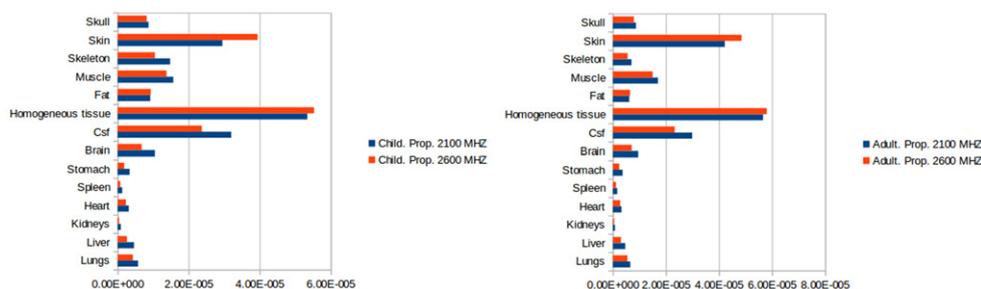
Figure 6. Comparison between local average SAR values obtained for child (left) and adult's (right) dielectric properties at different frequencies (2100 MHz in blue and 2600 MHz in red).

4.3.2. Influence of the dielectric properties on the whole-body and local average exposure of an 18 months child model. In order to study the importance of using age specific dielectric properties, we compared, for the 18 months child model, the whole-body, the maximum average and the local average exposure of the child model when using adult dielectric properties and 18 months old specific dielectric properties for the child model tissues at 2100 and 2600 MHz frequency bands. Table 5 presents the *WBSAR* and *SAR*10*g* results when performing the analysis with age-specific or adults tissue properties. As we can see, results are of the same order of magnitude and can be considered as equivalent for both frequency bands. Figures 5 and 6 present the results for the average local SAR values for both frequency bands. The actual numbers can be found in table 6. In both frequency bands, skin exposure is overestimated when using adult dielectric properties while fat exposure tends to be underestimated. As brain exposure is a major health concern, many epidemiological studies have focused on the relationship between EMF exposure and brain tumors and more particularly on the brain cumulative exposure to EMF (Aydin *et al* 2011, Cardis *et al* 2011a, 2011b). As we can see here, while

Table 6. Absolute power Pabs (W) and average local SAR (W kg^{-1}) values when using child specific dielectric properties (CDP) and adult dielectric properties (ADP) for the 18 months child model at 2100 and 2600 MHz.

Model	Tissue	2100 MHz		2600 MHz	
		Pabs	SAR	Pabs	SAR
Child's dielec. prop.	Lungs (1)	$1.63E-06$	$5.78E-06$	$1.22E-06$	$4.31E-06$
	Liver (2)	$1.11E-06$	$4.64E-06$	$6.30E-07$	$2.64E-06$
	Kidneys (3)	$4.36E-08$	$9.08E-07$	$2.03E-08$	$4.23E-07$
	Heart (4)	$4.14E-07$	$3.17E-06$	$3.05E-07$	$2.34E-06$
	Spleen (5)	$5.74E-08$	$1.31E-06$	$3.40E-08$	$7.76E-07$
	Stomach (6)	$2.31E-07$	$3.39E-06$	$1.26E-07$	$1.85E-06$
	Brain (7)	$9.23E-06$	$1.05E-05$	$5.95E-06$	$6.78E-06$
	CSF (8)	$2.16E-06$	$3.20E-05$	$1.60E-06$	$2.37E-05$
	Hom. tissues (9)	$1.42E-04$	$5.34E-05$	$1.47E-04$	$5.53E-05$
	Fat (10)	$2.93E-05$	$9.20E-06$	$2.97E-05$	$9.32E-06$
	Muscle (11)	$2.42E-05$	$1.57E-05$	$2.12E-05$	$1.38E-05$
	Skeleton (12)	$1.56E-05$	$1.48E-05$	$1.10E-05$	$1.05E-05$
	Skin (13)	$1.45E-05$	$2.95E-05$	$1.94E-05$	$3.94E-05$
	Skull (14)	$1.07E-05$	$8.72E-06$	$1.00E-05$	$8.20E-06$
Adult's dielec. prop.	Lungs (1)	$1.85E-06$	$6.57E-06$	$1.55E-06$	$5.50E-06$
	Liver (2)	$1.12E-06$	$4.68E-06$	$7.35E-07$	$3.08E-06$
	Kidneys (3)	$3.93E-08$	$8.19E-07$	$2.39E-08$	$4.97E-07$
	Heart (4)	$4.30E-07$	$3.29E-06$	$3.61E-07$	$2.76E-06$
	Spleen (5)	$7.38E-08$	$1.68E-06$	$5.22E-08$	$1.19E-06$
	Stomach (6)	$2.51E-07$	$3.68E-06$	$1.66E-07$	$2.43E-06$
	Brain (7)	$8.38E-06$	$9.55E-06$	$6.26E-06$	$7.13E-06$
	CSF (8)	$2.02E-06$	$2.99E-05$	$1.57E-06$	$2.33E-05$
	Hom. tissues (9)	$1.50E-04$	$5.66E-05$	$1.54E-04$	$5.80E-05$
	Fat (10)	$1.97E-05$	$6.20E-06$	$2.07E-05$	$6.51E-06$
	Muscle (11)	$2.61E-05$	$1.70E-05$	$2.30E-05$	$1.50E-05$
	Skeleton (12)	$7.42E-06$	$7.04E-06$	$5.88E-06$	$5.58E-06$
	Skin (13)	$2.07E-05$	$4.22E-05$	$2.39E-05$	$4.85E-05$
	Skull (14)	$1.07E-05$	$8.74E-06$	$9.69E-06$	$7.92E-06$

brain exposure tends to be underestimated when using adult dielectric properties at 2100 MHz (by about 10%), it is overestimated at 2600 MHz (by about 5%). These results highlight the need, when studying local exposure, to consider age specific dielectric properties.

5. Conclusion

In this paper, a segmentation and anatomy transfer based framework has been proposed, and new infant models to be used for numerical dosimetry simulations have been developed. The idea is to use registered segmented organs between a source model and a target model to guide the blind deformation of the other tissues. The segmented organs are obtained using a segmentation framework combining a new intensity-based energy and shape priors into a variational region growing

based method. This method allows for the simultaneous segmentation of multiple tissues. These tissues are then used in an anatomy transfer framework which incrementally adds new tissues to the target model and uses the newly registered tissues as constraints for the remaining ones. While the proposed method targets the early childhood, it is not specific to it and thus could be used for all possible ages, for instance for completing older children models such as those developed in Fouquier *et al* (2011). Using this method, five child models from 5 to 37 months containing thirteen tissues have been created. While artifacts such as slight deformations of the skull, imprecise positioning of the elbows and bending of muscle and fat still remain in the deformation procedure, the quality of the segmentation and following deformation procedure is good enough to ensure the production of realistic 3D anatomical models of the human body. The resulting models have thus been used to conduct a preliminary study on the exposure of 5 to 37 months old children models to radiofrequency electromagnetic fields from cellular base stations that are connecting the mobile phones to the networks. The first results show a decrease of the whole body exposure with age. Comparing exposure results obtained by using adult dielectric properties for the child tissues and those obtained by using child specific dielectric properties, we have seen that there is no influence of dielectric properties on the whole-body SAR and the average maximum over $10g$ SAR. In particular, when looking at the brain exposure, depending on the frequency band, the child brain exposure can be under- or over-estimated when using adult dielectric properties for the child tissues. This highlights the importance of using age-specific dielectric properties when studying children exposure. However, these results should be considered cautiously because of the combined uncertainties inherent to the estimation of the dielectric properties, models posturing and the variability in morphology.

Acknowledgments

Appendix. Tissues weights in kg per model

	5 months old	18 months old	37 months old
Lungs	0.19	0.28	0.315
Liver	0.188	0.23	0.335
Kidneys	0.028	0.04	0.06
Heart	0.1	0.13	0.14
Spleen	0.03	0.043	0.05
Stomach	0.02	0.068	0.08
Intestine	0.003	0.005	0.009
Brain	0.58	0.87	1.08
CSF	0.08	0.06	0.13
Hom. tissues	2.22	2.65	3.3
Fat	1.76	3.18	3.1
Muscle	1.84	1.537	2.67
Skeleton	0.77	1.05	1.42
Skin	0.36	0.49	0.58
Skull	0.477	1.22	0.73
Total	8.68	11.9	14.09

References

Achanta R, Shaji A, Smith K, Lucchi A, Fua P and Su S 2012 SLIC superpixels compared to state-of-the-art superpixel methods *IEEE Trans. Pattern Anal. Mach. Intell.* **34** 2274–82

Ali-Hamadi D, Liu T, Gilles B, Kavan L, Faure F, Palombi O and Cani M P 2013 Anatomy transfer *ACM Trans. Graph.* **32** 1–8

Aydin D *et al* 2011 Mobile phone use and brain tumors in children and adolescents: a multicenter case-control study *J. Natl Cancer Inst.* **103** 1264–76

Besl P J and Mckay H D 1992 A method for registration of 3D shapes *IEEE Trans. Pattern Anal. Mach. Intell.* **14** 239–56

Cardis E *et al* 2011a Risk of brain tumours in relation to estimated RF dose from mobile phones: results from five interphone countries *Occup. Environ. Med.* **68** 631–40

Cardis E *et al* 2011b Estimation of RF energy absorbed in the brain from mobile phones in the interphone study *Occup. Environ. Med.* **68** 686–93

Cassola V F, Kramer R, de Melo Lima V J, de Oliveira Lira C A B, Khoury H J, Vieira J W and Brown K R 2013 Development of newborn and 1 year old reference phantoms based on polygon mesh surfaces *J. Radiol. Prot.* **33** 669

Christ A *et al* 2010 The virtual family-development of surface-based anatomical models of two adults and two children for dosimetric simulations *Phys. Med. Biol.* **55** N23

Dahdouh S and Bloch I 2015 Shape-based multi-region segmentation framework: application to 3D infants MRI data *SPIE Medical Imaging (Orlando, FL, USA)* vol 413 pp 9941312-1–9941312-9

Dahdouh S, Varsier N, Serrurier A, la Plata J P D, Anquez J, Angelini E D, Wiart J and Bloch I 2014 A comprehensive tool for image-based generation of fetus and pregnant women mesh models for numerical dosimetry studies *Phys. Med. Biol.* **59** 4583–602

Duck F A 1990 *Physical Properties of Tissue. A Comprehensive Reference Book* (New York: Academic)

Faraj N, Thiery J M, Bloch I, Varsier N, Wiart J and Boubekeur T 2012 Robust and scalable interactive freeform modeling of high definition medical images *MICCAI Workshop on Mesh Processing in Medical Imaging* vol 7599 (New York: Springer) pp 1–11

Fouquier G, Anquez J, Bloch I, Falip C and Adamsbaum C 2011 Subcutaneous adipose tissue segmentation in whole-body MRI of children *CIARP (Chile)* vol 7042 pp 97–104

Gabriel C 2005 Dielectric properties of biological tissue: Variation with age *Bioelectromagnetics* **26** S12–8

Gabriel S, Lau R and Gabriel C 1996 The dielectric properties of biological tissues: II. Measurements in the frequency range 10 Hz to 20 GHz *Phys. Med. Biol.* **41** 2251

Gilles B, Reveret L and Pai D K 2010 Creating and animating subject-specific anatomical models *Comput. Graph. Forum* **29** 2340–51

Gosselin M C *et al* 2014 Development of a new generation of high-resolution anatomical models for medical device evaluation: the virtual population 3.0. *Phys. Med. Biol.* **59** 5287

Guy E, Thiery J M and Boubekeur T 2014 Simselect: similarity-based selection for 3D surfaces *Comput. Graph. Forum* **33** 165–73

Hadjem A, Lautru D, Dale C, Wong M F, Hanna V and Wiart J 2005 Study of specific absorption rate (SAR) induced in two child head models and in adult heads using mobile phones *IEEE Trans. Microw. Theory Tech.* **53** 4–11

Lee C, Lodwick D, Hasenauer D, Williams J L, Lee C and Bolch W E 2007 Hybrid computational phantoms of the male and female newborn patient: nurbs-based whole-body models *Phys. Med. Biol.* **52** 3309

Li C *et al* 2015 Generation of infant anatomical models for evaluating electromagnetic field exposures *Bioelectromagnetics* **36** 10–26

Müller M, Heidelberger B, Teschner M and Gross M 2005 Meshless deformations based on shape matching *ACM Trans. Graph.* **24** 471–8

Nagaoka T, Kunieda E and Watanabe S 2008 Proportion-corrected scaled voxel models for Japanese children and their application to the numerical dosimetry of specific absorption rate for frequencies from 30 MHz to 3 GHz *Phys. Med. Biol.* **53** 6695

Peyman A and Gabriel C 2010 Cole–Cole parameters for the dielectric properties of porcine tissues as a function of age at microwave frequencies *Phys. Med. Biol.* **55** N413–9

Peyman A, Rezazadeh A A and Gabriel C 2001 Changes in the dielectric properties of rat tissue as a function of age at microwave frequencies *Phys. Med. Biol.* **46** 1617

Revol-Muller C, Rose J, Pacureanu A, Peyrin F and Odet C 2012 Shape prior in variational region growing *Int. Conf. on Image Processing Theory, Tools and Applications* pp 116–20

Rose J, Revol-Muller C, Reichert C and Odet C 2009 Variational region growing *Int. Conf. on Computer Vision Theory and Applications* pp 166–71

Taflove A 2005 *Computational Electrodynamics: the Finite-Difference Time-Domain Method* 2nd edn (Boston, MA: Artech House)

Wiart J, Hadjem A, Wong M F and Bloch I 2008 Analysis of RF exposure in the head tissues of children and adults *Phys. Med. Biol.* **53** 3681–95

Xu X G and Eckerman K F 2009 *Handbook of Anatomical Models for Radiation Dosimetry* (Boca Raton, FL: CRC Press)

Zhu Y and Gortler S 2007 3D deformation using moving least squares *Technical Report* Cambridge MA